ADVANCES IN ATMOSPHERIC SCIENCES, VOL. 36, JANUARY 2019, 79–92

• **Original Paper** •

Subdaily to Seasonal Change of Surface Energy and Water Flux of the Haihe River Basin in China: Noah and Noah-MP Assessment

Fuqiang YANG[1,2], Li DAN*[1], Jing PENG[1], Xiujing YANG[1,2], Yueyue LI[2,3], and Dongdong GAO[4]

[1]*Key Laboratory of Regional Climate-Environment for Temperate East Asia, Institute of Atmospheric Physics, Chinese Academy of Sciences, Beijing* 100029*, China*

[2]*University of Chinese Academy of Sciences, Beijing* 100049*, China*

[3]*Institute of Geographical Sciences and Natural Resources Research, Chinese Academy of Sciences, Beijing* 100101*, China*

[4]*School of Atmospheric Sciences, Chengdu University of Information Technology, Chengdu* 610225*, China*

(Received 2 March 2018; revised 8 July 2018; accepted 31 July 2018)

ABSTRACT

The land surface processes of the Noah-MP and Noah models are evaluated over four typical landscapes in the Haihe River Basin (HRB) using in-situ observations. The simulated soil temperature and moisture in the two land surface models (LSMs) is consistent with the observation, especially in the rainy season. The models reproduce the mean values and seasonality of the energy fluxes of the croplands, despite the obvious underestimated total evaporation. Noah shows the lower deep soil temperature. The net radiation is well simulated for the diurnal time scale. The daytime latent heat fluxes are always underestimated, while the sensible heat fluxes are overestimated to some degree. Compared with Noah, Noah-MP has improved daily average soil heat flux with diurnal variations. Generally, Noah-MP performs fairly well for different landscapes of the HRB. The simulated cold bias in soil temperature is possibly linked with the parameterized partition of the energy into surface fluxes. Thus, further improvement of these LSMs remains a major challenge.

Key words: land surface model, Haihe River Basin, soil temperature, soil moisture, surface energy flux, seasonal cycle

Citation: Yang, F. Q., L. Dan, J. Peng, X. J. Yang, Y. Y, Li, and D. D. Gao, 2019: Subdaily to seasonal change of surface energy and water flux of the Haihe River Basin in China: Noah and Noah-MP assessment. *Adv. Atmos. Sci.*, **36**(1), 79–92, https://doi.org/10.1007/s00376-018-8035-4.

1. Introduction

The importance of land surface processes to weather and climate change has been increasingly recognized. The land surface regulates the partition of precipitation, evaporation, runoff or snowfall, and controls the terrestrial energy balance (Dickinson, 1995; Dan and Ji, 2007). As a result, the variation of surface available energy will directly affect the regional climate, hydrological change, and the carbon/nitrogen cycles (Dan et al., 2015; Peng and Dan, 2015). A key component to study land–atmosphere interactions and climate projections is land surface models (LSMs), which can be easily used to simulate the hydrological, biogeophysical, and biogeochemical processes (Chen et al., 2011). Rapid growth in LSM development has resulted in both the improvement of existing physical process representations and the addition of new processes and functions (Cai et al., 2014a). However, different LSMs vary in their levels of complexity and the types of physical parameterizations they incorporate, and differ in their outputs (Pitman, 2003). It is therefore important to evaluate and validate LSMs before using them to study land surface–atmosphere interactions in a particular region.

As a newly developed LSM, the multi-parameterization options version of the Noah model (Noah-MP) incorporates the recently improved physics in LSMs (Niu et al., 2011; Yang et al., 2011). Compared with other LSMs, it has been shown to present reasonable snow characteristics and surface heat fluxes in the Colorado forested region (Chen et al., 2014). Although, the authors of that study also highlighted that it remains a challenge to parameterize the cascading effect of the snow albedo, the canopy-scale turbulence, and radiative transfer. Moreover, Zheng et al. (2015) enhanced the multi-parameterization framework in representing the under-canopy turbulence transfer and root water uptake, and improved the model capacity to simulate the vertical profile of soil temperature and water. Recently, Zhang et al. (2016) used different analysis methods to identify the impacts of atmospheric forcing uncertainties, vegetation parameters, and subprocesses on the physics in Noah-MP ensemble simulations. They found that precipitation data uncertainty has a greater influence than that in leaf area index (LAI). Combining a

* Corresponding author: Li DAN
Email: danli@tea.ac.cn

better precipitation forcing dataset and monthly satellite retrievals of LAI significantly reduced the uncertainty range of the ensemble mean of surface heat fluxes. Ultimately, these offline simulation results all indicate that the worldwide use of the new community Noah-MP LSM still requires more rigorous assessments and validations, especially in China.

Eddy-covariance (EC) observations have been carried out in typical landscapes to investigate the water and energy balance in the Haihe River Basin (HRB). These kinds of observations are necessary to validate and improve LSM development (Jia et al., 2012; Liu et al., 2013). However, according to these studies, such assessments and validations of Noah-MP in the HRB are still limited, partly due to the lack of relevant observations. The objective of this study, therefore, is to assess the performance of Noah-MP in the HRB by simulating water and terrestrial fluxes in different typical landscapes of the region. For comparison, we also present the offline simulation results of version 3.4 of Noah. The data and methods used are described in section 2. Section 3 presents the validations of the Noah-MP and Noah model results with respect to corresponding observational data. Section 4 concludes the study, along with some further discussion.

2. Data and methods

2.1. *Observational data and sites*

The HRB is a semi-humid and semi-arid transitional region of China (Fig. 1). This region covers about 318 000 km^2, accounting for 3.3% of the national land area. With more than 10% of the national population in this region, including Beijing, Tianjin, and some other megacities, it has become one of the most densely populated areas of the world (Liu et al., 2013). The northern and western basin is dominated by mountains, accounting for about 60% of the whole domain, while the eastern and southeastern part is mainly distributed on the North China Plain. The annual average temperature ranges from 9.2°C to 13.5°C, and the total annual precipitation exceeds 400 mm, being spatial heterogeneous and concentrated in June to September (Table 1). With agricultural production generating a high water demand under the conditions of rapid economic development, over 12% of the satellite-detected increase in evapotranspiration can be attributed to human-induced activities in the region (Pan et al., 2017). Ultimately, investigating the water resources and analyzing the surface energy balance in this basin are important and urgent research topics.

Four experimental sites (Miyun, Huailai, Daxing and Guantao stations) established over typical landscapes were selected for the validation of the LSM (Table 1). Miyun and Huailai stations are located in the northern mountains of the basin. The maximum vegetation heights are 4.0 m for orchard (plum and apple trees) and 2.2 m for maize at Miyun station. Daxing station is situated in the middle reaches of the basin on suburban farmland. The maximum vegetation heights are 2.2, 0.7 and 0.5 m, for maize, winter wheat and vegetables, respectively. Guantao station is located in the southern North China Plain. The maximum vegetation heights are 2.2, 0.7

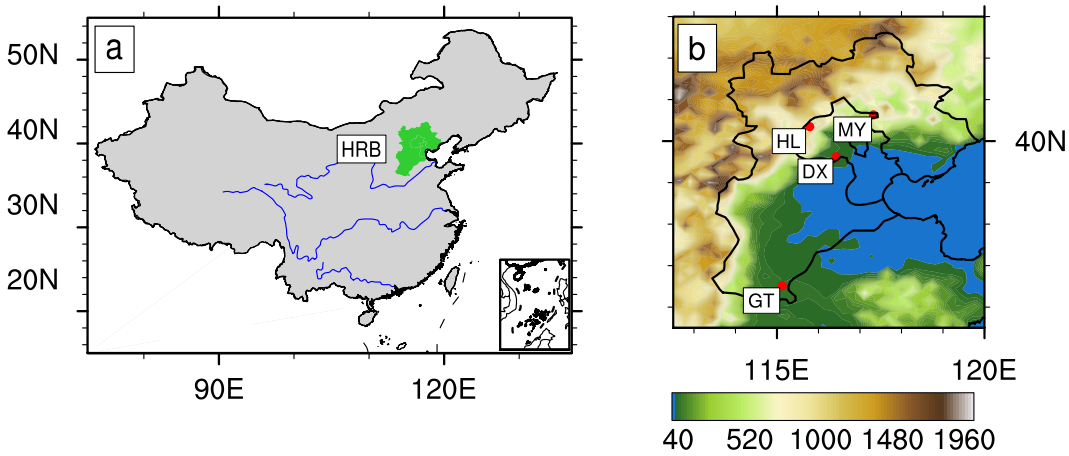

Fig. 1. The (a) location and (b) topography height of the HRB in China. The labels represent the flux sites as follows: MY, Miyun; HL, Huailai; DX, Daxing; GT, Guantao. The topography height (units: m) is color-shaded.

Table 1. Summary of the surface characteristics at the four validation sites.

Site	Latitude (°N)	Longitude (°E)	Time	MAT	MAP	Vegetation	Soil
MY	40.63	117.32	Jan 2008 – Dec 2010	9.2	486.8	Cropland/woodland mosaic	Loam
HL	40.35	115.79	Jan 2014 – Dec 2015	10.2	461.1	Dryland cropland and pasture	Clay loam
DX	39.62	116.43	Jul 2008 – Nov 2010	12.8	404.3	Irrigated cropland and pasture	Clay loam
GT	36.52	115.13	Oct 2009 – Dec 2010	13.5	577.9	Irrigated cropland and pasture	Sandy clay loam

Notes: MY, Miyun; HL, Huailai; DX, Daxing; GT, Guantao; MAT, mean annual temperature (°C); MAP, mean annual precipitation (mm).

and 1.2 m, for maize, winter wheat and cotton, respectively, around the site. The measurements of heat flux data were logged every 30 min, and the meteorological and soil thermal flux data were obtained from an automatic weather station (AWS) at 10 min intervals. Additional details about these sites and data processing are presented in Jia et al. (2012) and Liu et al. (2013).

2.2. *Noah*

The Noah LSM has been incorporated into the Weather Research and Forecasting (WRF) Model (Skamarock et al., 2008) and the NOAA/National Centers for Environmental Prediction weather/climate forecasting systems (Cai et al., 2014a). It is the most commonly used scheme in WRF applications at present. Basically, it has a vegetation canopy, one snow layer, and four soil layers with depths of 10, 30, 60 and 100 cm from the land surface to the bottom. The one-dimensional thermal diffusion formula is taken for the soil temperature calculation, and Richard's equation is adopted to predict the soil moisture:

$$\frac{\partial \rho_s C_s T}{\partial t} = \frac{\partial}{\partial z}\left(\lambda_s \frac{\partial T}{\partial z}\right); \tag{1}$$

$$\frac{\partial \theta}{\partial t} = \frac{\partial y}{\partial x}\left[D(\theta)\frac{\partial \theta}{\partial z}\right] + \frac{\partial K(\theta)}{\partial z} + S_s(\theta)\,. \tag{2}$$

Here, T is the soil temperature (K) and θ is the soil moisture content ($m^3\ m^{-3}$), t is the time interval (s), z is the soil depth (m), ρ_s is the soil density ($kg\ m^{-3}$), C_s is the soil heat capacity ($J\ kg^{-1}\ K^{-1}$), λ_s is the soil thermal conductivity ($W\ K^{-1}\ m^{-1}$), D is the soil water diffusivity ($m^2\ s^{-1}$), K is the hydraulic conductivity ($m\ s^{-1}$), and S_s represents the water sources and sinks (i.e., precipitation and evapotranspiration; $m\ s^{-1}$). The other parameters, such as LAI, minimum canopy resistance and roughness length, are prescribed (Rosero et al., 2010). A more detailed description of the model can be found in Chen and Dudhia (2001) and Chen et al. (2010).

2.3. *Noah-MP*

Building on the original Noah model (Ek et al., 2003), Noah-MP was enhanced through the addition of improved physics and employing an ensemble forecasting framework (Niu et al., 2011; Yang et al., 2011). The improved physics includes dynamic groundwater, an interactive vegetation canopy, and a multi-layer snowpack. In contrast with Noah (version 3.0), Niu et al. (2011) used enhanced physical schemes and improved the runoff and surface flux simulations of steppe. Using the fully augmented version of Noah-MP, Yang et al. (2011) also showed improvements in soil water, runoff and skin temperature simulations, across river basins worldwide.

The multi-parameterization options provide users with multiple choices of parameterizations in leaf dynamics, canopy stomatal resistance, and soil moisture factors for stomatal resistance, runoff and groundwater. Each combination of these different parameter scheme options could form an ensemble forecasting. The total number of combinations of the 10 multiple parameterization options described in Niu et al. (2011) can be up to 4608, representing 4608 alternative schemes. Given the regional climate characteristics and computational demand, we selected five major processes that might significantly affect land surface interactions in the HRB, which resulted in 144 ensemble experiments. These selected five major parameterization options include (1) canopy stomatal resistance, (2) soil moisture factors for stomatal resistance, (3) runoff and groundwater, (4) surface layer drag coefficient, and (5) radiation transfer. Details on the other aspects of the model can be found in Niu et al. (2011) and Zhang et al. (2016), while the ensemble mean of these 144 process parameterizations will be analyzed in this study.

2.4. *Experimental design*

Four experiments with the Noah and Noah-MP LSMs were implemented at Miyun, Huailai, Daxing, and Guantao stations, independently. While the integrations did not take into consideration the dynamic vegetation process, due to the relatively short simulation period, the green vegetation fraction and LAI were prescribed. The soil textures were classified as loam for the Miyun run, clay loam for the Daxing and Huailai runs, and sandy clay loam for the Guantao run, based on the Food and Agriculture Organization database. The vegetation types were cropland/woodland mosaic for the Miyun run, dryland cropland and pasture for the Huailai run, and irrigated cropland and pasture for the Daxing and Guantao runs, according to U.S. Geological Survey classification (Table 1).

The atmospheric forcing data were downloaded directly from a multiscale surface flux and meteorological elements observation dataset in the HRB, which includes precipitation, air temperature, atmospheric relative humidity, downward short- and longwave radiation, surface pressure, and wind speed. All the abovementioned EC and AWS data were rigorously and carefully processed following uniform standard procedures (Jia et al., 2012). Gaps in the forcing data, which were generally no more than few hours, were filled by linear interpolation. Each offline simulation was initialized by repeating the forcing data 50 times to ensure soil moisture and temperature convergence was achieved. Given the observational data availability, the offline LSMs were integrated from January 2008 to December 2010 at Miyun station, from January 2014 to December 2015 at Huailai station, from July 2008 to November 2010 at Daxing station, and from October 2009 to December 2010 at Guantao station.

The simulated seasonal variations of soil temperature, soil moisture, net radiation, surface energy fluxes, and soil heat flux were validated. At the same time, we also analyzed the diurnal uncertainties of the surface heat fluxes for boreal summer (June through August) and winter (December through February). The biases of the models are depicted by the Pearson correlation coefficient (COR), root-mean-square error (RMSE), and the mean bias error (MBE):

$$\mathrm{MBE} = \frac{1}{N}\sum_{i=1}^{N}(M_i - O_i)\,; \tag{3}$$

$$\mathrm{RMSE} = \sqrt{\frac{\sum_{i=1}^{N}(M_i - O_i)^2}{N}}. \quad (4)$$

Here, M_i and O_i are the daily averages of the simulation and observation for the ith day, and N is the number of days.

The mean energy balance ratios are 0.80, 0.86, 0.76 and 0.93 for Miyun, Daxing, Huailai and Guantao stations, respectively. Since the EC data always show energy imbalance, the surface heat fluxes could be underestimated. The Bowen ratio (Bo = H/LE, where H is the sensible heat flux and LE is the latent heat flux) energy closure method was used to adjust the sensible and latent heat flux on a daily basis (Twine et al., 2000; Liu et al., 2013). The corrected fluxes were only utilized to explore the seasonal and interannual variations at the corresponding observation station (here, we utilized the flux adjustment on daily aggregated fluxes instead of invoking flux correction at every half-hour time step, to avoid errors due to high-frequency flux variations).

3. Results

3.1. *Simulation at Miyun*

3.1.1. *Daily soil temperature and moisture*

The soil temperature was validated at the depth of 10 and 40 cm for Miyun station (Fig. 2). Generally, the soil temperatures are underestimated in the two LSMs. The discrepancies between Noah-MP outputs and observations are slight when the simulation begins, suggesting that the discrepancy might be linked with sensor calibration errors. The shallow soil layer shows more consistency between simulations and observations than that of the deep soil layer, as revealed by lower MBE values (Table 2). The soil temperature is underestimated by approximately 1.00°C in the upper soil layer, and by about 2.00°C in the deeper soil layer. Compared with Noah-MP, Noah shows more bias, with RMSE of approximately 2.76°C in the shallow soil layer and 3.57°C in the deeper soil layer. The warm season soil temperatures are overestimated, while the cold season soil temperatures are underestimated, especially for the deeper soil layer, in Noah. This result is inconsistent with previous studies (Jin et al., 1999; Chen et al., 2014), possibly because of our physics process selections. Given the semi-humid and semi-arid transitional climate in the HRB (annual average temperature ranges from 9.2°C to 13.5°C), we did not take into consideration snow processes and supercooled liquid water parameterizations. This may have resulted in underestimations of the winter soil temperature at this station. Although Noah treats the canopy and snow physics simply, it shows comparable performance with other more complicated LSMs (Niu et al., 2011; Cai et al., 2014a; Chen et al., 2014).

Figures 2c and d present the simulated and observed soil

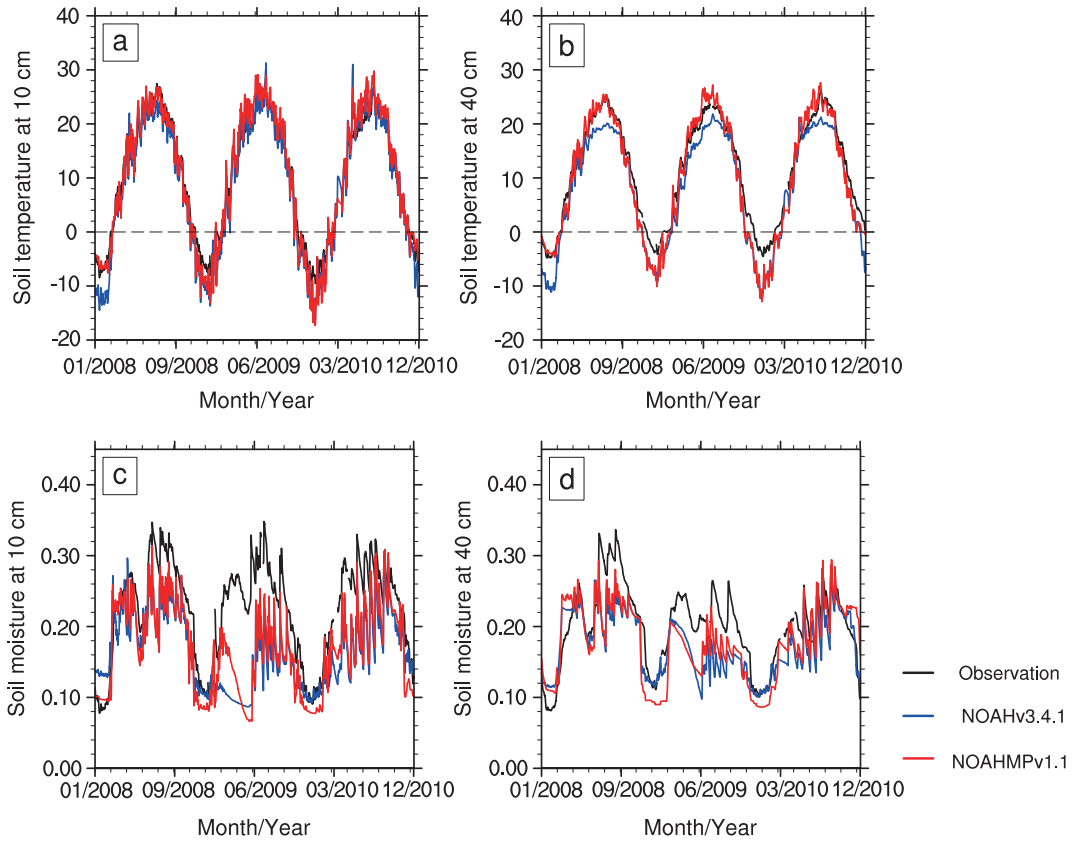

Fig. 2. Daily average (a, b) soil temperature and (c, d) soil moisture at depths of 10 cm and 40 cm from the Miyun run. The black lines are observations, the red lines are the Noah-MP LSM simulations, and the blue lines are the Noah LSM simulations. The units are °C for soil temperature and $m^3\ m^{-3}$ for soil moisture.

Table 2. Statistics of daily averaged soil temperature and soil moisture at the depth of 10 cm and 40 cm, net radiation, turbulent heat fluxes, and soil heat flux from Miyun station.

	Noah-MP			Noah		
	COR	MBE	RMSE	COR	MBE	RMSE
Soil temperature at 10 cm	0.99	−0.17	2.42	0.99	−1.53	2.76
Soil temperature at 40 cm	0.98	−1.26	2.75	0.99	−3.18	3.57
Soil moisture at 10 cm	0.75	−0.06	0.07	0.61	−0.06	0.08
Soil moisture at 40 cm	0.76	−0.02	0.04	0.75	−0.03	0.04
Net radiation	0.98	−10.94	17.94	0.98	−3.05	11.74
Latent heat flux	0.84	−12.26	31.58	0.86	−13.84	31.57
Sensible heat flux	0.51	−15.48	32.43	0.56	−4.58	28.72
Soil heat flux	0.85	−0.97	7.34	0.84	−1.75	6.98

Notes: all correlation coefficients passed the 95% confidence test. The MBE and RMSE are in °C.

wetness at the depths of 10 and 40 cm at Miyun station. Precipitation is a key contributor to the seasonal variations of soil moisture in this region. In summer, when most rainfall events are concentrated, the soil moisture shows large daily variations. In winter, fewer rainfall events take place and the soil moisture fluctuations are stable. Noah-MP and Noah capture the seasonal variations of soil moisture reasonably well. Although there are some dry biases in both LSM simulations, it is clear that Noah-MP is closer to the observational situation (MBE = −0.06 and −0.02 m^3 m^{-3} at the 10 and 40 cm soil layer, respectively). In the summer rainy season, Noah-MP shows potential skill to decrease the dry soil moisture discrepancy of the original Noah LSM. It should be mentioned that the soil moisture simulations in both LSMs are apparently smaller than the observations in 2009 at Miyun station (Fig. 2c). This is probably related to in-situ forcing measurements missed during several rainfall events before the summer period (not shown).

3.1.2. *Surface energy fluxes*

The daily averages of the latent heat flux, sensible heat flux, net radiation, and soil heat flux at the Miyun site are presented in Fig. 3. It can be seen that the offline simulations successfully capture the seasonal variations of surface heat fluxes, although the simulated results are smaller than in-situ observations during some periods. The net radiation heat flux is the major proportion in land–atmosphere energy exchange, which is the best simulated flux component by both LSMs (COR = 0.98). Noah-MP underestimates the daily sensible and latent heat flux (MBE around 10 W m^{-2}), while Noah shows more comparable sensible heat flux with the observation (Table 2). At the same time, both LSMs capture well the seasonal variations of the ground heat flux.

The simulated energy fluxes were also compared with ob-

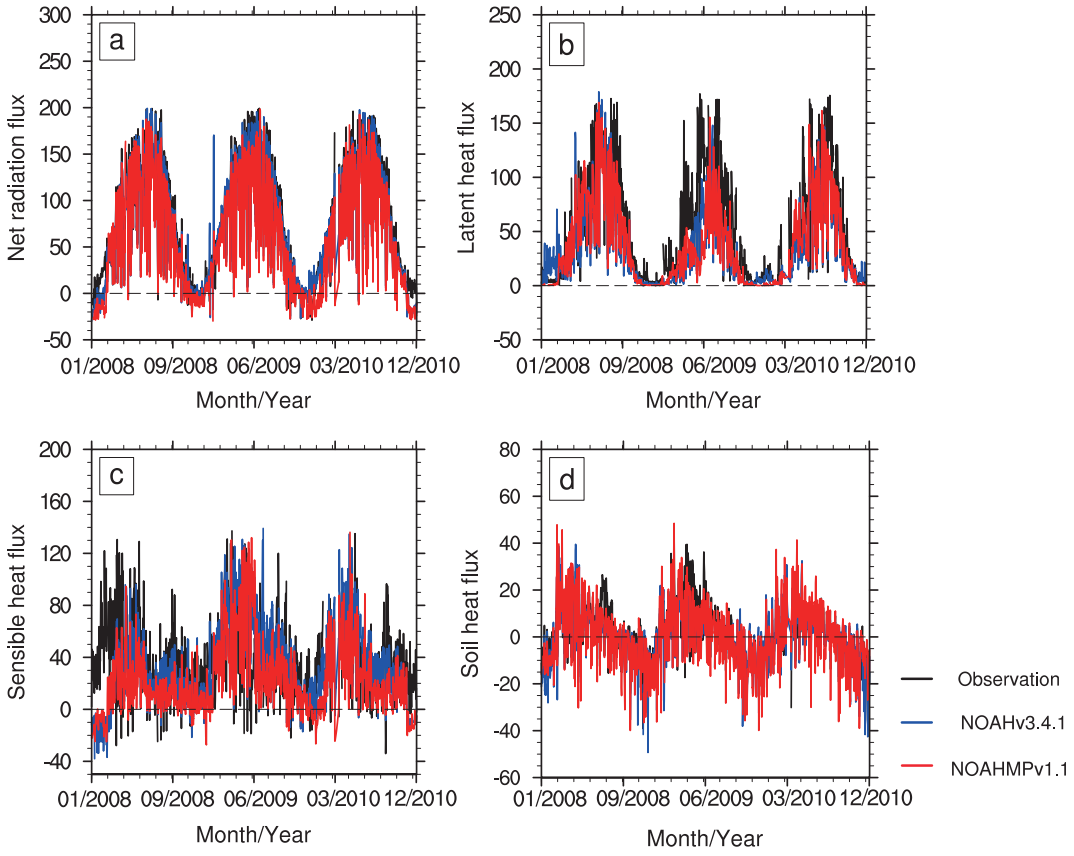

Fig. 3. Daily average (a) net radiation, (b) latent heat flux, (c) sensible heat flux, and (d) soil heat flux at Miyun station. The black lines are tower observations, the red lines are the Noah-MP LSM simulations, and the blue lines are the Noah LSM simulations. Units: W m^{-2}.

servations in terms of half-hour averages to investigate the diurnal cycle. At Miyun station, larger variations of the surface energy flux could be found in the daytime than at nighttime (Fig. 4). In summer daytime, the two LSMs underestimate the net radiation and total evaporation. Compared with Noah, Noah-MP obviously improves the sensible heat flux simulation in the daytime. While Noah captures the diurnal variations of the soil heat fluxes in summer well, Noah-MP overestimates the daytime soil heat fluxes and underestimates them at nighttime. This is probably due to the different parameterization process for surface soil thermal conductivity (Niu et al., 2011). Due to the model structural change (i.e., separating the vegetation canopy from the soil surface), Noah-MP removes the exponential decay of the surface soil thermal diffusivity with vegetation cover fraction (Peters-Lidard et al., 1998), which was adopted by the original Noah LSM. The performances of the LSMs in winter are similar to the summer situation. The daytime net radiation and sensible heat flux are underestimated to some degree.

On average, annually, the diurnal variations of the surface water flux are reasonably reproduced by both LSMs. The two LSMs underestimate the net radiation but overestimate the sensible heat flux during the daytime. Compared with Noah, Noah-MP improves the thermal flux simulation during the daytime and shows more daily fluctuations of soil heat flux simulation. To summarize, the diurnal variations of the sensible heat flux, net radiation and latent heat flux from both LSMs are reasonably captured in terms of the annual daily average at Miyun station (Fig. 4). The ground heat flux is overestimated, which might be linked to the parameterization algorithm of leaf stomata in croplands (De Gonçalves et al., 2013).

3.2. *Simulation at Huailai*

3.2.1. *Daily soil temperature and moisture*

As with Miyun station, the simulated daily soil temperatures at the depths of 10 and 40 cm were validated at Huailai station (Fig. 5). Generally, the LSM simulations show similar seasonal patterns to the AWS data products, with correlation coefficients ranging from 0.89 to 0.99 and RMSE ranging from 4.14°C to 5.66°C (Table 3). However, a warm soil temperature bias exists in the two soil layers in both LSMs. In particular, the simulated warm soil temperature deviations at 40 cm can reach up to 10.0°C in summer. Compared with Noah (MBE = 4.57°C and 0.27°C at 10 and 40 cm, respectively), using Noah-MP exaggerates the warm deviations (MBE = 5.75°C and 1.77°C).

The daily mean observed and simulated soil moisture at Huailai station at the depths of 10 and 40 cm are presented in Figs. 5c and d. Although both LSMs capture the seasonal variations of soil moisture in both soil layers, there are always some wet simulation discrepancies, especially in winter. This

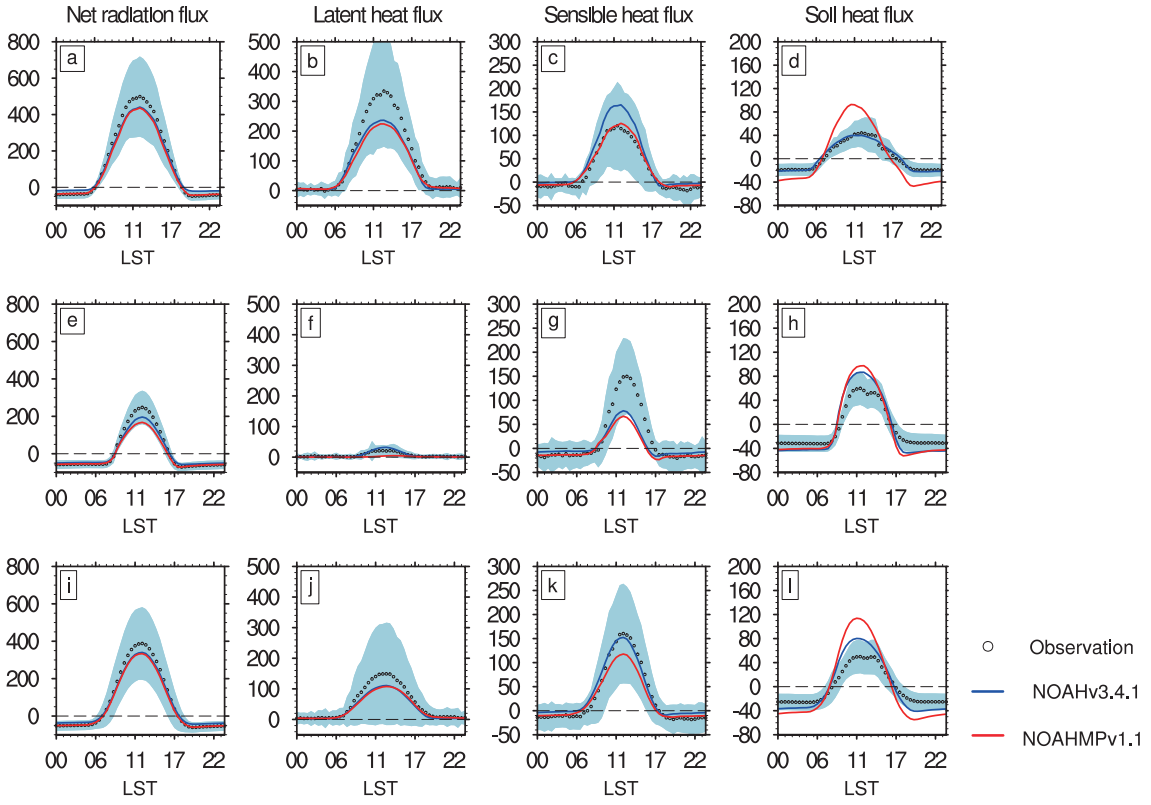

Fig. 4. Diurnal cycle of (a, e, i) net radiation, (b, f, j) latent heat flux, (c, g, k) sensible heat flux, and (d, h, l) soil heat flux for the Miyun run during the (a–d) summer, (e–h) winter, and (i–l) annual average. The black circles are tower observations, the red lines are the Noah-MP LSM simulations, and the blue lines are the Noah LSM simulations. Units: W m^{-2}. The light-blue shaded region indicates ±1 standard deviations of variation for half-hourly tower observations.

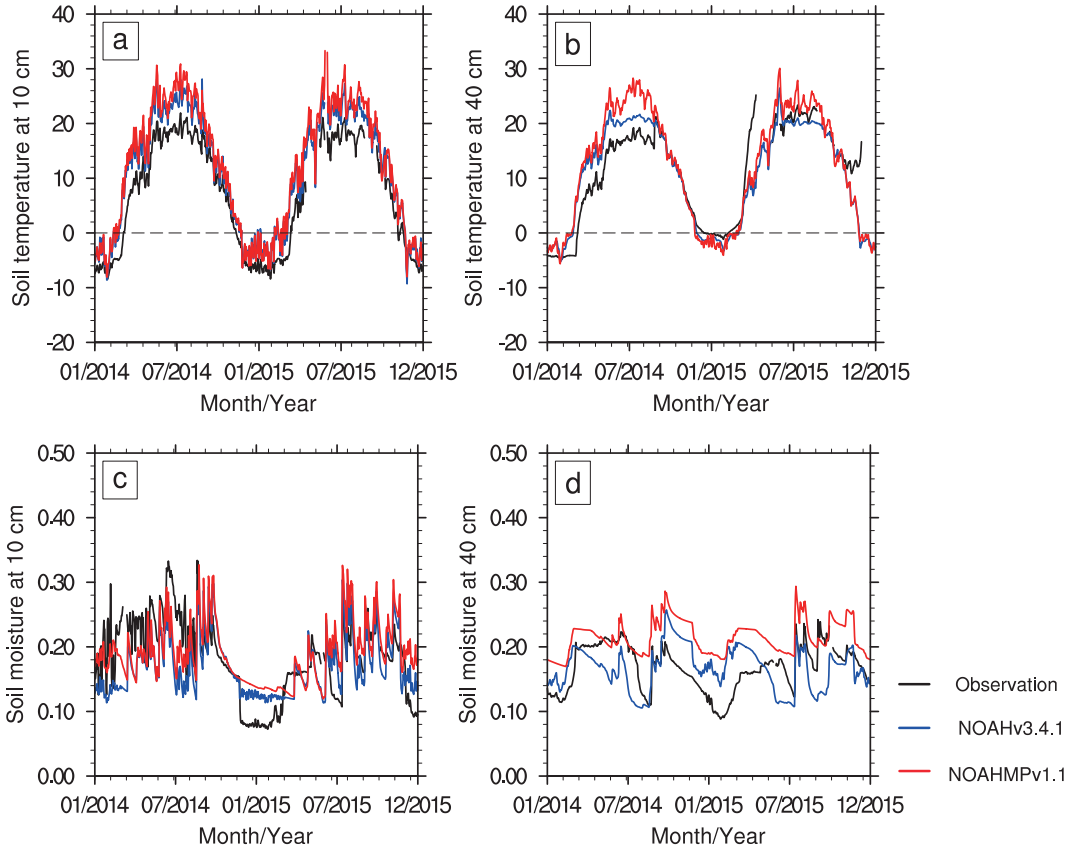

Fig. 5. As in Fig. 2 but for Huailai station.

Table 3. As in Table 2 but for Huailai station.

	Noah-MP			Noah		
	COR	MBE	RMSE	COR	MBE	RMSE
Soil temperature at 10 cm	0.98	5.75	5.66	0.99	4.57	4.41
Soil temperature at 40 cm	0.89	1.77	5.22	0.89	0.27	4.14
Soil moisture at 10 cm	0.58	0.01	0.05	0.58	−0.01	0.05
Soil moisture at 40 cm	0.57	0.05	0.06	0.20	−0.00	0.04
Net radiation	0.97	−5.00	15.88	0.99	−1.72	9.92
Latent heat flux	0.77	−13.95	30.85	0.81	−13.77	30.80
Sensible heat flux	0.49	4.12	33.68	0.53	9.25	35.61
Soil heat flux	0.77	−0.98	8.29	0.73	−1.32	6.73

Notes: all correlation coefficients passed the 95% confidence test. The MBE and RMSE are in °C.

is probably related to the simple snowfall treatments and snowmelt parameterizations in the LSMs (Chen et al., 2014). Compared with the shallow soil layer (10 cm), the soil moisture variations at the deeper soil layer (40 cm) are significantly improved by Noah-MP compared with Noah.

3.2.2. *Surface energy fluxes*

The daily average net radiation, latent heat flux, sensible heat flux, and soil heat flux at Huailai station are shown in Fig. 6. During the warm summer, the magnitudes and daily variations of the turbulent heat fluxes are large. The two LSMs adequately capture the seasonal variations of the soil heat flux and net radiation. The sensible heat flux is overestimated to some extent, while the latent heat flux is underestimated by both offline simulations in the cold season (Table 3).

Figure 7 presents the simulated and observed diurnal cycle of surface energy heat fluxes at Huailai station. The net radiation with hourly variation is reasonably simulated by the two LSMs. The water flux is underestimated, while the sensible heat is overestimated in the daytime, especially in the warmer rainy season (Fig. 7c). The surface net radiation is simulated well in the two LSMs, with the bias in the partition of surface heat fluxes. It should be noted that the diurnal variations of soil heat flux for both LSMs are larger than the original in-situ data. In other words, when compared with the observational data, the LSMs absorb more radiation energy from the sun in the daytime, while they release more radiation flux to the atmosphere at night. This situation is even more serious for Noah-MP in summer.

3.3. *Simulation at Daxing*

3.3.1. *Daily soil temperature and moisture*

The simulated daily soil temperature and moisture at the depths of 10 and 40 cm at Daxing station were validated against observations (Fig. 8). Generally, the LSMs appropriately capture the seasonal variations of the soil temperatures, with correlation coefficients ranging from 0.96 to 0.97 (Table 4). However, the simulated soil temperature magnitudes

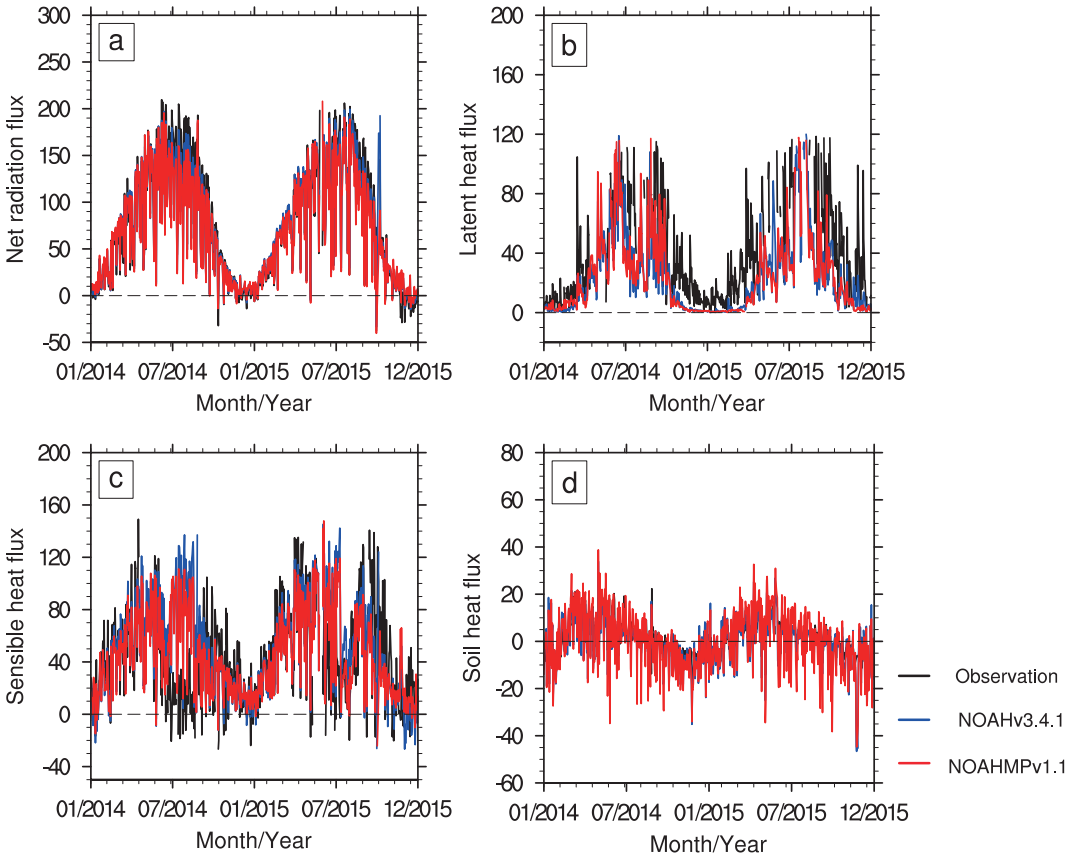

Fig. 6. As in Fig. 3 but for Huailai station.

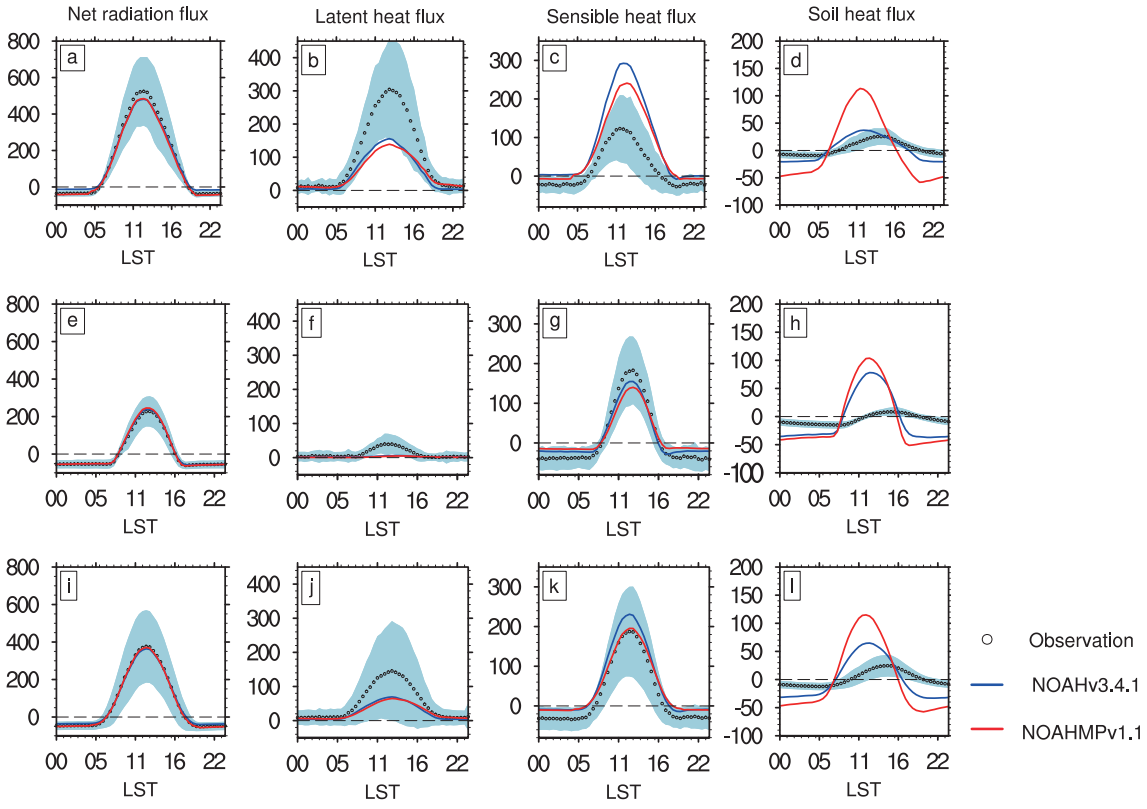

Fig. 7. As in Fig. 4 but for Huailai station.

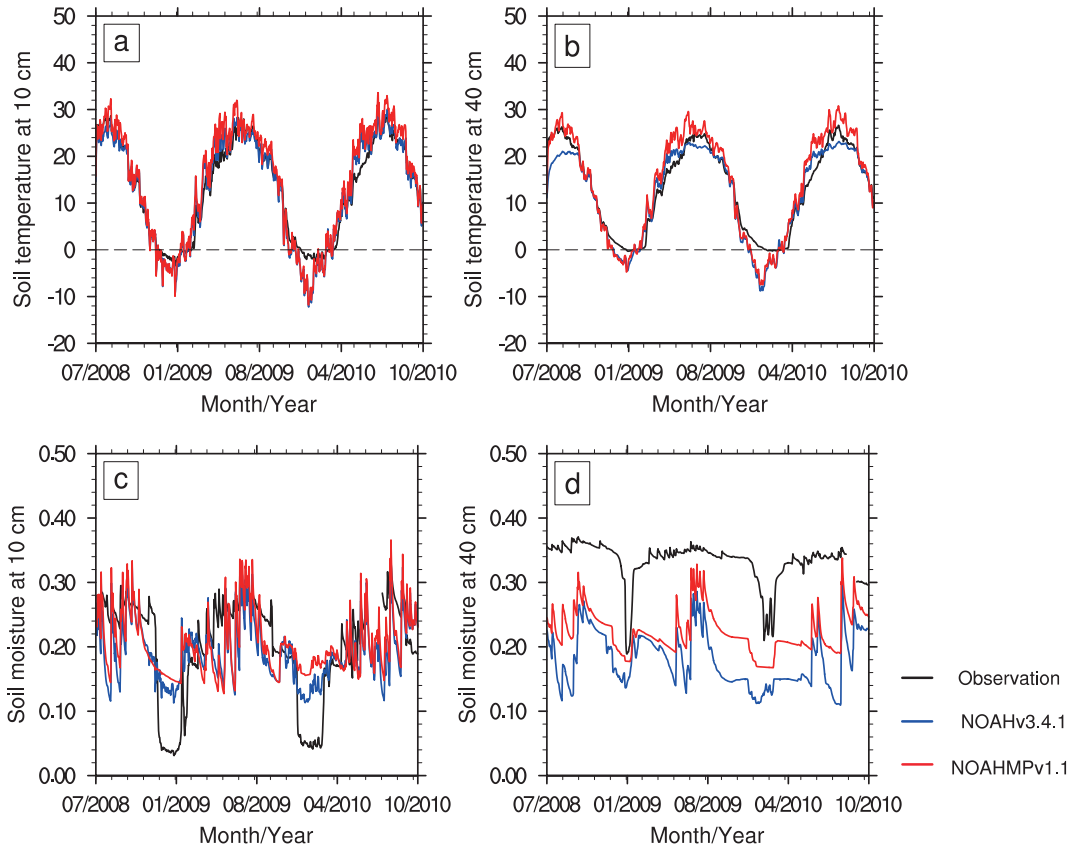

Fig. 8. As in Fig. 2 but for Daxing station.

Table 4. As in Table 2 but for Daxing station.

	Noah-MP			Noah		
	COR	MBE	RMSE	COR	MBE	RMSE
Soil temperature at 10 cm	0.97	1.19	3.40	0.97	−0.12	2.71
Soil temperature at 40 cm	0.97	1.12	3.20	0.96	−0.94	2.82
Soil moisture at 10 cm	0.56	0.00	0.07	0.63	−0.01	0.06
Soil moisture at 40 cm	0.52	−0.11	0.11	0.34	−0.15	0.16
Net radiation	0.99	−2.98	10.05	0.99	−3.05	10.74
Latent heat flux	0.67	−31.60	48.04	0.72	−32.91	48.02
Sensible heat flux	0.28	−2.62	30.15	0.30	0.17	29.19
Soil heat flux	0.78	−0.44	8.09	0.75	−0.24	8.01

Notes: all correlation coefficients passed the 95% confidence test. The MBE and RMSE are in °C.

are much larger than the observed data (with RMSE ranging from 2.71°C to 3.40°C). The offline simulations always present higher (lower) soil temperatures in summer (winter) than the observations. This phenomenon is even distinct in the deeper soil layer. It is important to note that Noah-MP shows some improved skill in the summer soil temperature simulations, while the winter soil temperature simulations are comparable with Noah (Fig. 8b).

Soil moisture is underestimated in both LSMs' offline simulations (Table 4). While only the cold season moisture at the top soil layer is underestimated, a significant dry discrepancy is found at the deep soil layer throughout the whole simulation period in both LSMs, especially the baseline of Noah. Those differences could be partly related to the quality control of validation records and the soil hydraulic parameterization calibration that we did not consider. At the same time, the irrigation and runoff parameterization of the LSMs might also be key factor for soil moisture simulations (Yang et al., 2011). Future improvements in these aspects of modeling are essential as the next step.

3.3.2. *Surface energy fluxes*

Figure 9 presents the simulated and observed daily mean surface energy heat fluxes at Daxing station. It can be seen that all of the heat flux components are underestimated in both offline LSMs (Table 4). While the daily average of the soil heat and net radiation are adequately represented, both offline models always underestimate the latent heat flux (MBE around 30 W m^{-2}). The sensible heat is the worst surface energy component simulated by these two LSMs at this station.

Figure 10 exhibits the diurnal cycle of the simulated and observed energy and water heat fluxes at the Daxing site. In summer, Noah-MP and Noah capture the diurnal variations of latent heat flux and net radiation. The sensible heat flux is more likely to be overestimated by these two LSMs in summer daytime. Noah-MP improves the simulation of soil heat flux in the daytime, but brings more uncertainties, while Noah always underestimates the daytime soil heat flux. It should be noted that the irrigation process might play a more im-

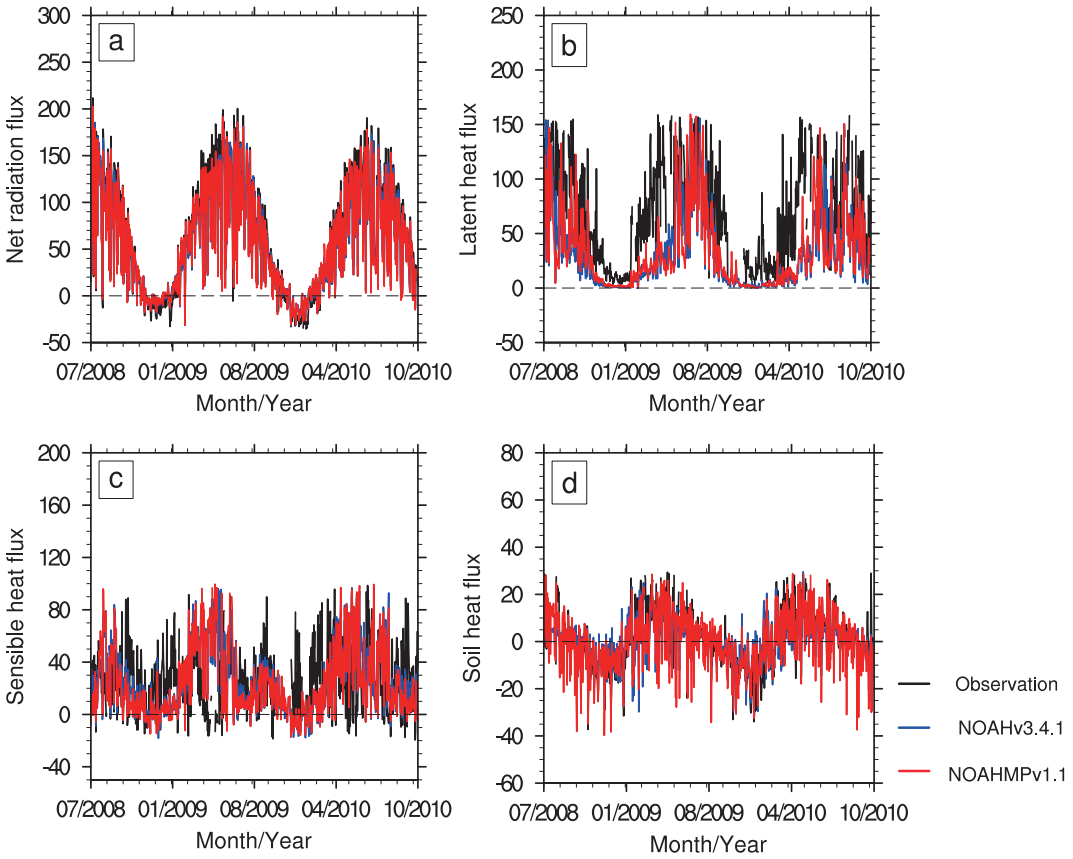

Fig. 9. As in Fig. 3 but for Daxing station.

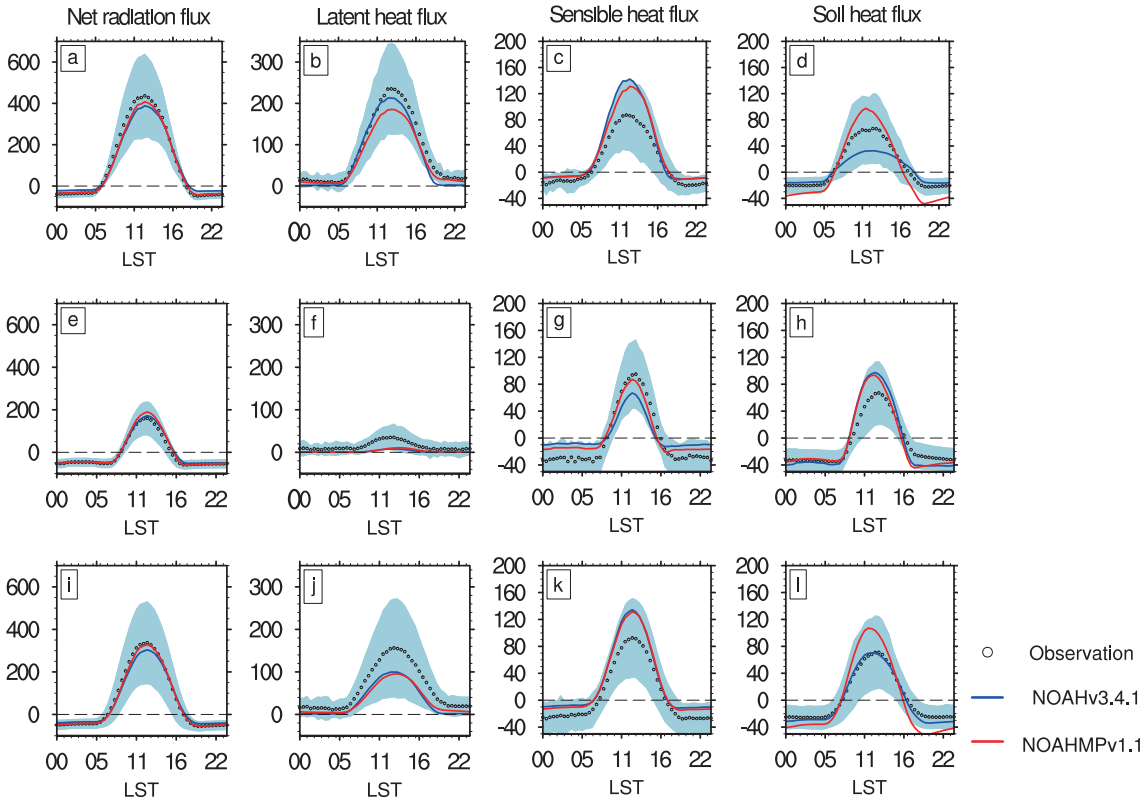

Fig. 10. As in Fig. 4 but for Daxing station.

portant role in this region than any other places because we always observe water evaporation even after sunset in winter (Fig. 10f). Since we did not consider any physical irrigation parameterization in this study, these two LSMs both significantly underestimate the winter latent heat fluxes. In terms of the annual average (Figs. 10i–l), both LSMs enhance the sensible heat and reduce the water flux in the daytime. While both LSMs reasonably capture the diurnal variations of soil heat flux and net radiation, Noah-MP also brings more uncertainties in soil heat flux simulations.

3.4. *Simulation at Guantao*

3.4.1. *Daily soil temperature and moisture*

Figure 11 shows the simulated and observed time series of daily mean soil temperature and soil moisture at Guantao station. It can be seen that the simulated soil temperature at 10 cm depth generally agrees with the observation in summer (Fig. 11a). However, the winter soil temperature simulation often shows cooler discrepancies, especially in the deeper soil layer (40 cm). Corresponding to soil temperature, both LSMs show similar performance in their soil moisture simulations. Considering the missing measurements through spring 2010, the LSMs capture more daily soil moisture variations at the shallow layer than at the deeper layer (Table 5).

3.4.2. *Surface energy fluxes*

The simulated and observed daily mean surface fluxes at Guantao station are illustrated in Fig. 12. The soil heat flux and net radiation simulations generally agree with the observations with respect to the magnitude and seasonal variations. However, the sensible and latent heat flux seem to show more discrepancies. In particular, distinctly underestimated latent heat could be found in both LSMs (Table 5). Noah LSM underestimates the sensible heat flux (MBE = −1.94 W m^{-2}), while Noah-MP shows slight improvements (MBE = −0.04 W m^{-2}).

Figure 13 presents the diurnal cycle of energy and water flux simulations and observations for the Guantao site. Both LSMs reasonably simulate the diurnal cycle of soil heat flux and net radiation. Compared to Noah LSM, the daytime latent heat flux is more realistically simulated by Noah-

Table 5. As in Table 2 but for Guantao station.

	Noah-MP			Noah		
	COR	MBE	RMSE	COR	MBE	RMSE
Soil temperature at 10 cm	0.99	−1.52	2.84	0.99	−2.52	3.05
Soil temperature at 40 cm	0.97	−0.46	3.42	0.97	−1.84	3.00
Soil moisture at 10 cm	0.70	−0.03	0.05	0.76	−0.03	0.05
Soil moisture at 40 cm	0.43	−0.05	0.06	0.38	−0.06	0.07
Net radiation	0.99	−4.56	12.74	0.99	−5.22	12.38
Latent heat flux	0.86	−11.13	24.35	0.84	−9.71	25.65
Sensible heat flux	0.48	0.04	22.46	0.43	−1.94	21.75
Soil heat flux	0.86	0.09	7.34	0.82	−0.21	7.32

Notes: all correlation coefficients passed the 95% confidence test. The MBE and RMSE are in °C.

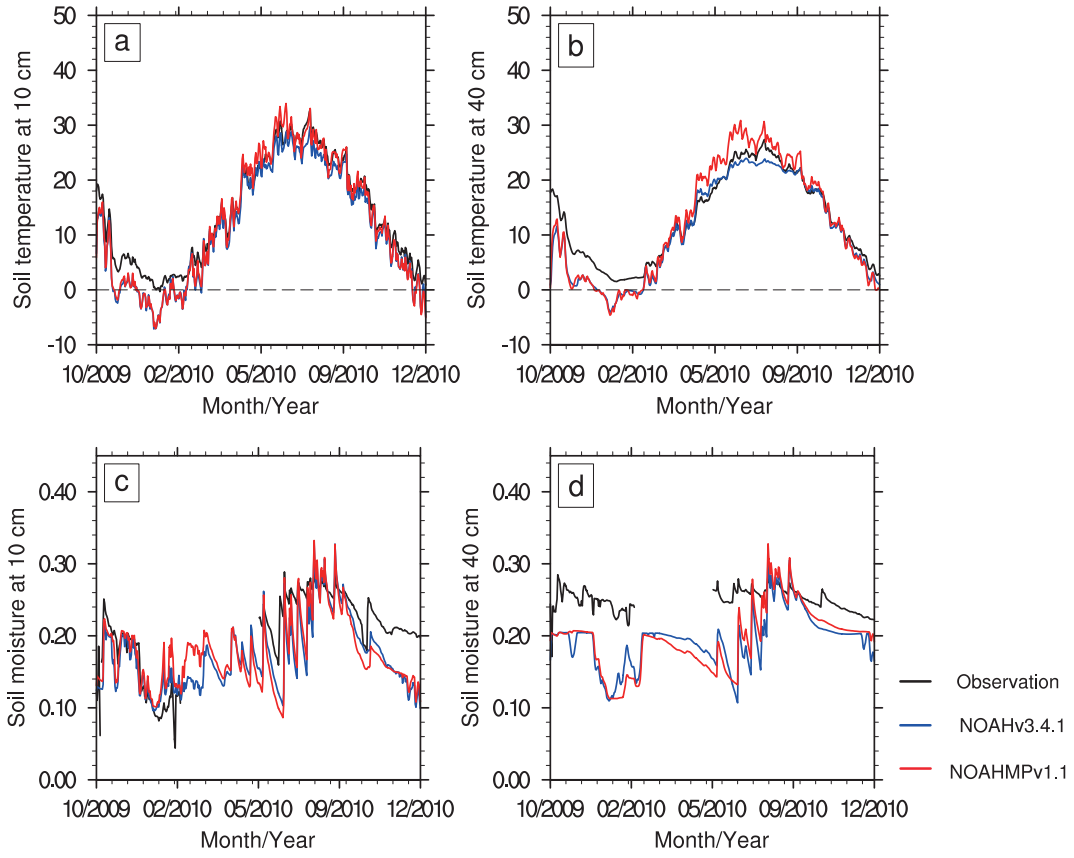

Fig. 11. As in Fig. 2 but for Guantao station.

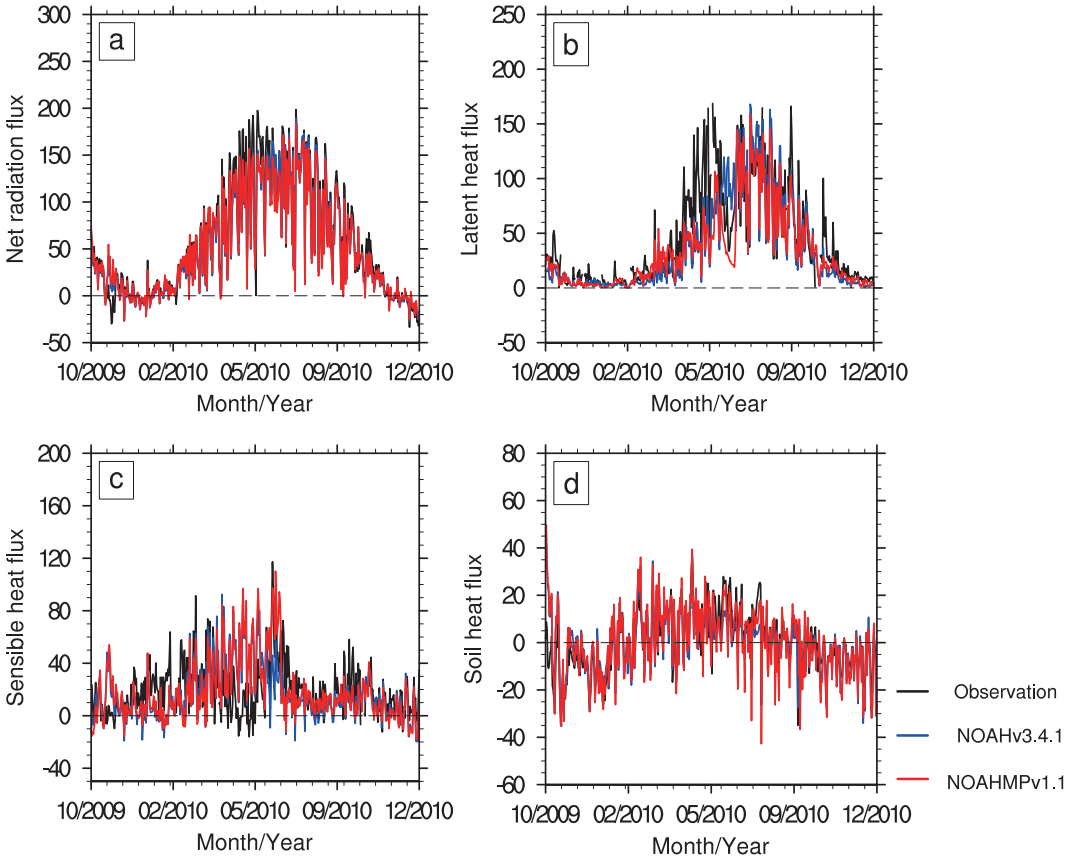

Fig. 12. As in Fig. 3 but for Guantao station.

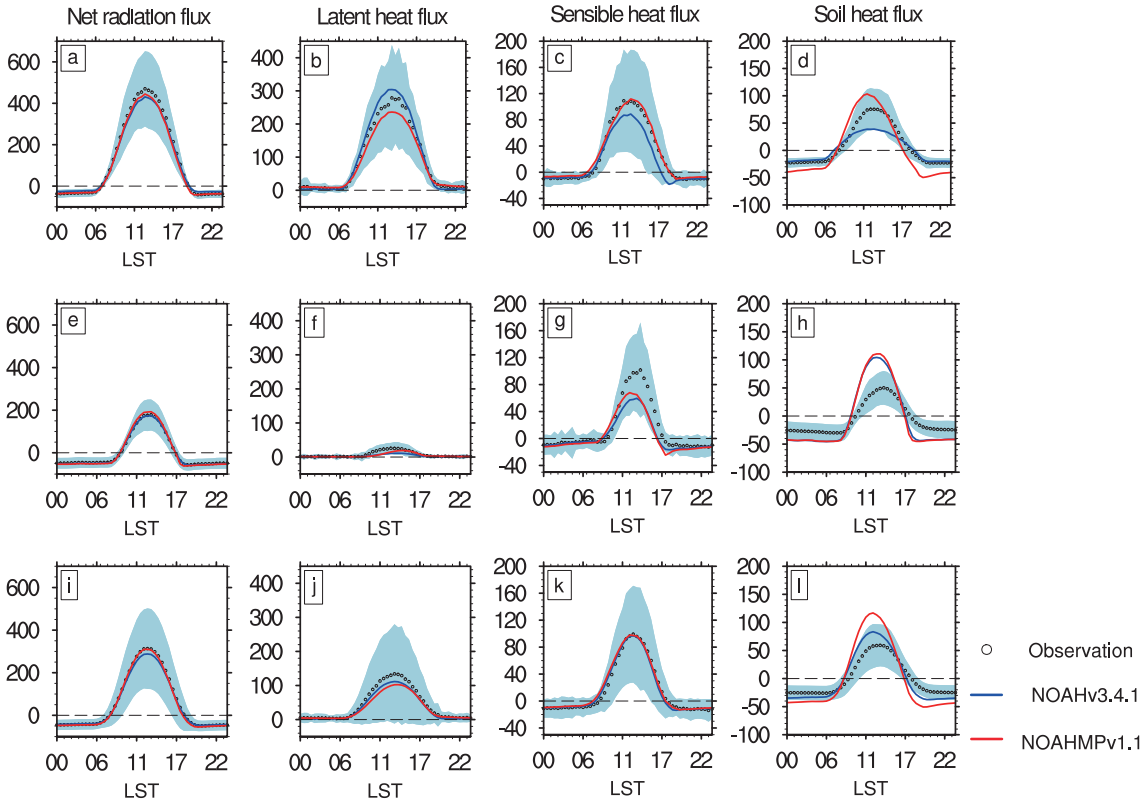

Fig. 13. As in Fig. 4 but for Guantao station.

MP, while the sensible heat flux is overestimated to some extent in summer (Figs. 13b and c). In winter, both LSMs correctly capture the sensible heat and net radiation, while the soil heat flux is overestimated and latent heat is partly underestimated. In terms of the annual average, these two offline LSMs reasonably predict the diurnal variation of the surface heat fluxes. The daytime latent heat flux is underestimated, while the sensible and soil heat flux are overestimated from sunrise to sunset. The simulated phase of soil heat flux diurnally leads that of the observations slightly at Guantao station.

4. Conclusions and discussion

Offline simulations of the Noah-MP and Noah LSMs were performed over four typical landscapes in the HRB of China. The model results were found to satisfactorily represent the seasonality of daily mean soil temperature, particularly in the warm periods, with correlation coefficients beyond 0.88. Both LSMs always show a cold bias in winter soil temperature simulations. These biases might be partly attributable to the model adjustment in simulating the equilibrium between the soil temperature and water. An LSM needs simultaneous water balance and energy closure. Such closure, however, brings difficulty for soil temperature and moisture simulations in LSMs (e.g., Pilotto et al., 2015). Due to the simplified parameterization of the runoff and snowfall processes, the soil moisture seasonal variations are harder to represent in offline runs. While the simulations of heat fluxes are comparable with the original Noah LSM, Noah-MP improves the soil moisture simulations to some extent.

The simulated soil moisture and temperature discrepancies increase with soil depth. This is possibly related to the offline model using constant soil parameter values along with the vertical soil profile, whereas hydraulic variations of soil exist in measurements (e.g., Yang et al., 2005; Gao et al., 2015). Organic matter is plentiful in the top soil layer, and thus it might also induce more uncertainties in the model results. Chen et al. (2012) pointed out that high soil organic carbon contained in the upper soil layer will weaken the bulk density and thermal conductivity but enhance the soil porosity.

Both LSMs reasonably capture the seasonal variations of surface energy flux. At the diurnal time scale, the net radiation components are the best simulated heat flux components. The daytime latent heat fluxes are always underestimated, while the sensible heat fluxes are overestimated to some degree. Compared with Noah, Noah-MP improves the daily average soil heat flux simulation, even with more diurnal variations. According to Blyth et al. (2010) and Cai et al. (2014b), the simulation is better for forest and grassland in Noah-MP, but the two LSMs both show larger latent heat in cropland. This might be attributable to the hard growth reproduction of crops by LAI in these two LSMs (Cai et al., 2014b). The crop submodel should be incorporated into the Noah LSM to represent the biogeophysical processes (Gayler et al., 2014).

This work shows a satisfactory capacity of Noah-MP to present the daily average and seasonal variations of surface energy flux in the HRB; however, the soil temperature simulations still exhibit some discrepancies. On the other hand, some uncertainties or biases of surface flux measurements (e.g., Twine et al., 2000; Yang and Wang, 2008) may still exist, due to our simple data processing and parameterization selection. Finally, these offline evaluations demonstrate that essential model improvements for heat and water simulations are needed. Evaluation of model performance over a fuller spectrum of parameter space (Gulden et al., 2008) should be conducted in the future.

Acknowledgements. This study was supported by a project of the National Key Research and Development Program of China (Grant No. 2016YFA0602501), a project of the National Natural Science Foundation of China (Grant Nos. 41630532 and 41575093). The dataset was provided by the Cold and Arid Regions Science Data Center at Lanzhou (http://westdc.westgis.ac.cn). We gratefully acknowledge Prof. Shaomin LIU of Beijing Normal University for providing the Haihe multiscale surface flux and meteorological elements observational experiments.

REFERENCES

Blyth, E., J. Gash, A. Lloyd, M. Pryor, G. P. Weedon, and J. Shuttleworth, 2010: Evaluating the JULES land surface model energy fluxes using FLUXNET data. *Journal of Hydrometeorology*, **11**(2), 509–519, https://doi.org/10.1175/2009JHM1183.1.

Cai, X. T., Z.-L. Yang, Y. L. Xia, M. Y. Huang, H. L. Wei, L. R. Leung, and M. B. Ek, 2014a: Assessment of simulated water balance from Noah, Noah-MP, CLM, and VIC over CONUS using the NLDAS test bed. *J. Geophys. Res.*, **119**(24), 13 751–13 770, https://doi.org/10.1002/2014JD022113.

Cai, X. T., Z.-L. Yang, C. H. David, G.-Y. Niu, and M. Rodell, 2014b: Hydrological evaluation of the Noah-MP land surface model for the Mississippi River Basin. *J. Geophys. Res.*, **119**(1), 23–38, https://doi.org/10.1002/2013JD020792.

Chen, F., and J. Dudhia, 2001: Coupling an advanced land surface-hydrology model with the Penn state-NCAR MM5 modeling system. Part I: model implementation and sensitivity. *Mon. Wea. Rev.*, **129**(4), 569–585, https://doi.org/10.1175/1520-0493(2001)129<0569:CAALSH>2.0.CO;2.

Chen, F., and Coauthors, 2014: Modeling seasonal snowpack evolution in the complex terrain and forested Colorado Headwaters region: a model intercomparison study. *J. Geophys. Res.*, **119**(24), 13 795–13 819, https://doi.org/10.1002/2014JD022167.

Chen, H. S., R. E. Dickinson, Y. J. Dai, and L. M. Zhou, 2011: Sensitivity of simulated terrestrial carbon assimilation and canopy transpiration to different stomatal conductance and carbon assimilation schemes. *Climate Dyn.*, **36**(5), 1037–1054, https://doi.org/10.1007/s00382-010-0741-2.

Chen, Y. Y., K. Yang, D. G. Zhou, J. Qin, and X. F. Guo, 2010: Improving the Noah land surface model in arid regions with an appropriate parameterization of the thermal roughness length. *Journal of Hydrometeorology*, **11**(4), 995–1006,

https://doi.org/10.1175/2010JHM1185.1.

Chen, Y. Y., K. Yang, W. J. Tang, J. Qin, and L. Zhao, 2012: Parameterizing soil organic carbon's impacts on soil porosity and thermal parameters for Eastern Tibet grasslands. *Science China Earth Sciences*, **55**(6), 1001–1011, https://doi.org/10.1007/s11430-012-4433-0.

Dan, L., and J. J. Ji, 2007: The surface energy, water, carbon flux and their intercorrelated seasonality in a global climate-vegetation coupled model. *Tellus B: Chemical and Physical Meteorology*, **59**(3), 425–438, https://doi.org/10.1111/j.1600-0889.2007.00274.x.

Dan, L., F. Q. Cao, and R. Gao, 2015: The improvement of a regional climate model by coupling a land surface model with eco-physiological processes: a case study in 1998. *Climatic Change*, **129**(3–4), 457–470, https://doi.org/10.1007/s10584-013-0997-8.

De Gonçalves, L. G. G., and Coauthors, 2013: Overview of the large-scale biosphere-atmosphere experiment in Amazonia data model intercomparison project (LBA-DMIP). *Agricultural and Forest Meteorology*, **182–183**, 111–127, https://doi.org/10.1016/j.agrformet.2013.04.030.

Dickinson, R. E., 1995: Land-atmosphere interaction. *Rev. Geophys.*, **33**(S2), 917–922, https://doi.org/10.1029/95RG00284.

Ek, M. B., K. E. Mitchell, Y. Lin, E. Rogers, P. Grunmann, V. Koren, G. Gayno, and J. D. Tarpley, 2003: Implementation of Noah land surface model advances in the National Centers for Environmental Prediction operational mesoscale eta model. *J. Geophys. Res.*, **108**(D22), 8851, https://doi.org/10.1029/2002jd003296.

Gao, Y. H., K. Li, F. Chen, Y. S. Jiang, and C. G. Lu, 2015: Assessing and improving Noah-MP land model simulations for the central Tibetan Plateau. *J. Geophys. Res.*, **120**(18), 9258–9278, https://doi.org/10.1002/2015JD023404.

Gayler, S., and Coauthors, 2014: Incorporating dynamic root growth enhances the performance of Noah-MP at two contrasting winter wheat field sites. *Water Resour. Res.*, **50**(2), 1337–1356, https://doi.org/10.1002/2013WR014634.

Gulden, L. E., E. Roseroe, Z. L. Yang, T. Wagener, and G. Y. Niu, 2008: Model performance, model robustness, and model fitness scores: a new method for identifying good land-surface models. *Geophys. Res. Lett.*, **35**(11), L11404, https://doi.org/10.1029/2008gl033721.

Jia, Z. Z., S. M. Liu, Z. W. Xu, Y. J. Chen, and M. J. Zhu, 2012: Validation of remotely sensed evapotranspiration over the Hai River Basin, China. *J. Geophys. Res.*, **117**(D13), D13113, https://doi.org/10.1029/2011JD017037.

Jin, J., X. Gao, Z.-L. Yang, R. C. Bales, S. Sorooshian, R. E. Dickinson, S. F. Sun, and G. X. Wu, 1999: Comparative analyses of physically based snowmelt models for climate simulations. *J. Climate*, **12**(8), 2643–2657, https://doi.org/10.1175/1520-0442(1999)012<2643:CAOPBS>2.0.CO;2.

Liu, S. M., Z. W. Xu, Z. L. Zhu, Z. Z. Jia, and M. J. Zhu, 2013: Measurements of evapotranspiration from eddy-covariance systems and large aperture scintillometers in the Hai River Basin, China. *J. Hydrol.*, **487**, 24–38, https://doi.org/10.1016/j.jhydrol.2013.02.025.

Niu, G.-Y., and Coauthors, 2011: The community Noah land surface model with multiparameterization options (Noah-MP): 1. Model description and evaluation with local-scale measurements. *J. Geophys. Res.*, **116**(D12), D12109, https://doi.org/10.1029/2010JD015139.

Pan, Y., C. Zhang, H. L. Gong, P. J.-F. Yeh, Y. J. Shen, Y. Guo, Z. Y. Huang, and X. J. Li, 2017: Detection of human-induced evapotranspiration using GRACE satellite observations in the Haihe River basin of China. *Geophys. Res. Lett.*, **44**(1), 190–199, https://doi.org/10.1002/2016GL071287.

Peng, J., and L. Dan, 2015: Impacts of CO_2 concentration and climate change on the terrestrial carbon flux using six global climate-carbon coupled models. *Ecological Modelling*, **304**, 69–83, https://doi.org/10.1016/j.ecolmodel.2015.02.016.

Peters-Lidard, C. D., E. Blackburn, X. Liang, and E. F. Wood, 1998: The effect of soil thermal conductivity parameterization on surface energy fluxes and temperatures. *J. Atmos. Sci.*, **55**(7), 1209–1224, https://doi.org/10.1175/1520-0469(1998)055<1209:TEOSTC>2.0.CO;2.

Pilotto, I. L., D. A. Rodríguez, J. Tomasella, G. Sampaio, and S. C. Chou, 2015: Comparisons of the Noah-MP land surface model simulations with measurements of forest and crop sites in Amazonia. *Meteor. Atmos. Phys.*, **127**(6), 711–723, https://doi.org/10.1007/s00703-015-0399-8.

Pitman, A. J., 2003: The evolution of, and revolution in, land surface schemes designed for climate models. *International Journal of Climatology*, **23**(5), 479–510, https://doi.org/10.1002/joc.893.

Rosero, E., Z.-L. Yang, T. Wagener, L. E. Gulden, S. Yatheendradas, and G.-Y. Niu, 2010: Quantifying parameter sensitivity, interaction, and transferability in hydrologically enhanced versions of the Noah land surface model over transition zones during the warm season. *J. Geophys. Res.*, **115**(D3), D03106, https://doi.org/10.1029/2009JD012035.

Skamarock, W. C., and Coauthors, 2008: A description of the advanced research WRF version 3. NCAR Technical Note, NCAR/TN-475+STR, 125 pp.

Twine, T. E., and Coauthors, 2000: Correcting eddy-covariance flux underestimates over a grassland. *Agricultural and Forest Meteorology*, **103**(3), 279–300, https://doi.org/10.1016/S0168-1923(00)00123-4.

Yang, K., and J. M. Wang, 2008: A temperature prediction-correction method for estimating surface soil heat flux from soil temperature and moisture data. *Science in China Series D: Earth Sciences*, **51**(5), 721–729, https://doi.org/10.1007/s11430-008-0036-1.

Yang, K., T. Koike, B. S. Ye, and L. Bastidas, 2005: Inverse analysis of the role of soil vertical heterogeneity in controlling surface soil state and energy partition. *J. Geophys. Res.*, **110**(D8), D08101, https://doi.org/10.1029/2004JD005500.

Yang, Z.-L., and Coauthors, 2011: The community Noah land surface model with multiparameterization options (Noah-MP): 2. Evaluation over global river basins. *J. Geophys. Res.*, **116**(D12), D12110, https://doi.org/10.1029/2010JD015140.

Zhang, G., F. Chen, and Y. J. Gan, 2016: Assessing uncertainties in the Noah-MP ensemble simulations of a cropland site during the Tibet Joint International Cooperation program field campaign. *J. Geophys. Res.*, 121(16), 9576–9596, https://doi.org/10.1002/2016JD024928.

Zheng, D. H., R. Van Der Velde, Z. B. Su, J. Wen, M. J. Booij, A. Y. Hoekstra, and X. Wang, 2015: Under-canopy turbulence and root water uptake of a Tibetan meadow ecosystem modeled by Noah-MP. *Water Resour. Res.*, **51**(7), 5735–5755, https://doi.org/10.1002/2015wr017115.